Analytica Chimica Acta 1226 (2022) 340261

Contents lists available at ScienceDirect

Analytica Chimica Acta

journal homepage: www.elsevier.com/locate/aca

Differentiation of closely related mineral phases in Mars atmosphere using frequency domain laser-induced plasma acoustics

César Alvarez-Llamas [a,1], Pablo Purohit [a,b,1], Javier Moros [a], Javier Laserna [a,*]

[a] UMALaserLab, Departamento de Química Analítica, Universidad de Málaga, Jiménez Fraud 4, 29010, Málaga, Spain
[b] Niels Bohr Institute, University of Copenhagen, Blegdamsvej 17, 2100, Copenhagen, Denmark

HIGHLIGHTS

- Laser-induced plasma shockwave generate sample-specific optical and acoustic signal.
- A pathway for extracting analytical information from frequency domain is presented.
- Different minerals were differentiated by frequency-based chemometric models.
- The methodologies were evaluated under Mars conditions to test their general applicability.

GRAPHICAL ABSTRACT

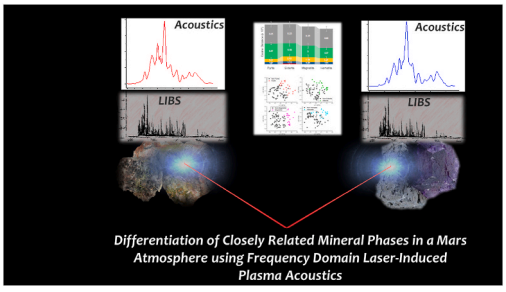

ARTICLE INFO

Keywords:
LIBS
Minerals
Laser-induced acoustics
Frequency domain
PLS
Mars

ABSTRACT

The combination of data yielded by laser-induced breakdown spectroscopy (LIBS) and laser-induced plasma acoustics (LIPAc) is a topic of many prospective applications as these coexisting phenomena can cover different sample traits. Among the most interesting features that LIPAc could add to the expanded target picture is information concerning structure and geophysical characteristics elusive to LIBS. In the present work, frequency spectra of minerals were explored to discriminate between chemically similar mineralogical phases. Several replicas of four different Fe-based minerals were analyzed to identify spectral traits linked to their chemistry in the frequency domain. First, the similarity between replicas of the same mineral family was verified and then, the cosine and Euclidian distances to minerals of different species were calculated to evaluate the discrimination capabilities of frequency spectra with results being compared to those obtained by LIBS. A partial least-squares *one-vs-all* model is described seeking to demonstrate sample classification by frequency means exclusively. As the use of LIBS-LIPAc for in-field mineral sorting has sparked interest, experiments reported were performed in stand-off within a thermal vacuum chamber (TVC). The TVC allowed data acquisition under Earth and Mars-like conditions, with the latter serving as a test of high relevance to assess the general applicability of the conclusions reached in Earth environment. Thorough discussion of data treatment is included with a focus on the impact of interference patterns arising from the laser-induced shockwave interaction with the medium surrounding the sample to avoid non-sample related information in the data processing schemes.

* Corresponding author.,
E-mail address: laserna@uma.es (J. Laserna).
[1] These authors contributed equally and are joint first authors.

https://doi.org/10.1016/j.aca.2022.340261
Received 10 May 2022; Received in revised form 15 July 2022; Accepted 11 August 2022
Available online 16 August 2022

1. Introduction

A major advantage displayed by analytical tools based on the interaction of the target sample with pulsed laser light is the numerous sources of information generated within a single inspection event [1,2]. By implementing multiple detection devices, simultaneous data revealing different sample traits can provide a more complete and extensive description of the target. As an analytical tool, LIBS has displayed exceptional synergy for merging with other techniques; such as LIBS and Raman analysis, thus resulting in a complete elemental and molecular study of the sample [3,4].

Recently, attention has been directed towards unraveling information regarding the physicochemical traits of solid samples contained in the acoustic shockwave accompanying the formation of laser-induced plasmas. The detection of the laser-induced acoustic signal has been used to LIBS normalization [5] or to estimate the ablated mass removed after a laser ablation event [6]. In the last few years, LIPAc is undergoing a hyperactivity period boosted by the NASA M2020 mission's Perseverance rover, which includes a microphone that can be synchronized to the LIBS laser in the SuperCam instrument [7,8]. Several studies have been performed to study how the physical properties of minerals impact the emitted acoustic wave; demonstrating that the wave acoustic energy and its variation are related to properties such as Vickers hardness, ablation rate or mineral phase [9–12]. Furthermore, studies exploiting the acoustic signal in time domain demonstrated the collaboration between LIBS and laser-induced acoustics to improve the overall analytical performance [13].

In the present work, the laser-induced acoustic response of four different Fe-rich mineral families is studied in the frequency domain alongside their optical emission spectra. The main objective of the work is to evaluate whether recorded frequencies contain mineral phase-related information that can provide complementary data to the optical results. To do so, replicas of the same mineral family were inspected to evaluate the existence of features in the acoustic spectra particular only to a given mineral.

The recorded acoustic spectra dissimilarity degree was calculated using cosine and Euclidean distances. Discrimination potential using exclusively acoustic frequencies is studied using PCA and PLS *one-vs-all* models and compared to LIBS. Experiments performed herein were carried in remote configuration and under Earth and Mars atmospheric conditions to showcase the generality of the conclusions drawn for the studies and the feasibility of their application in a scenario of interest.

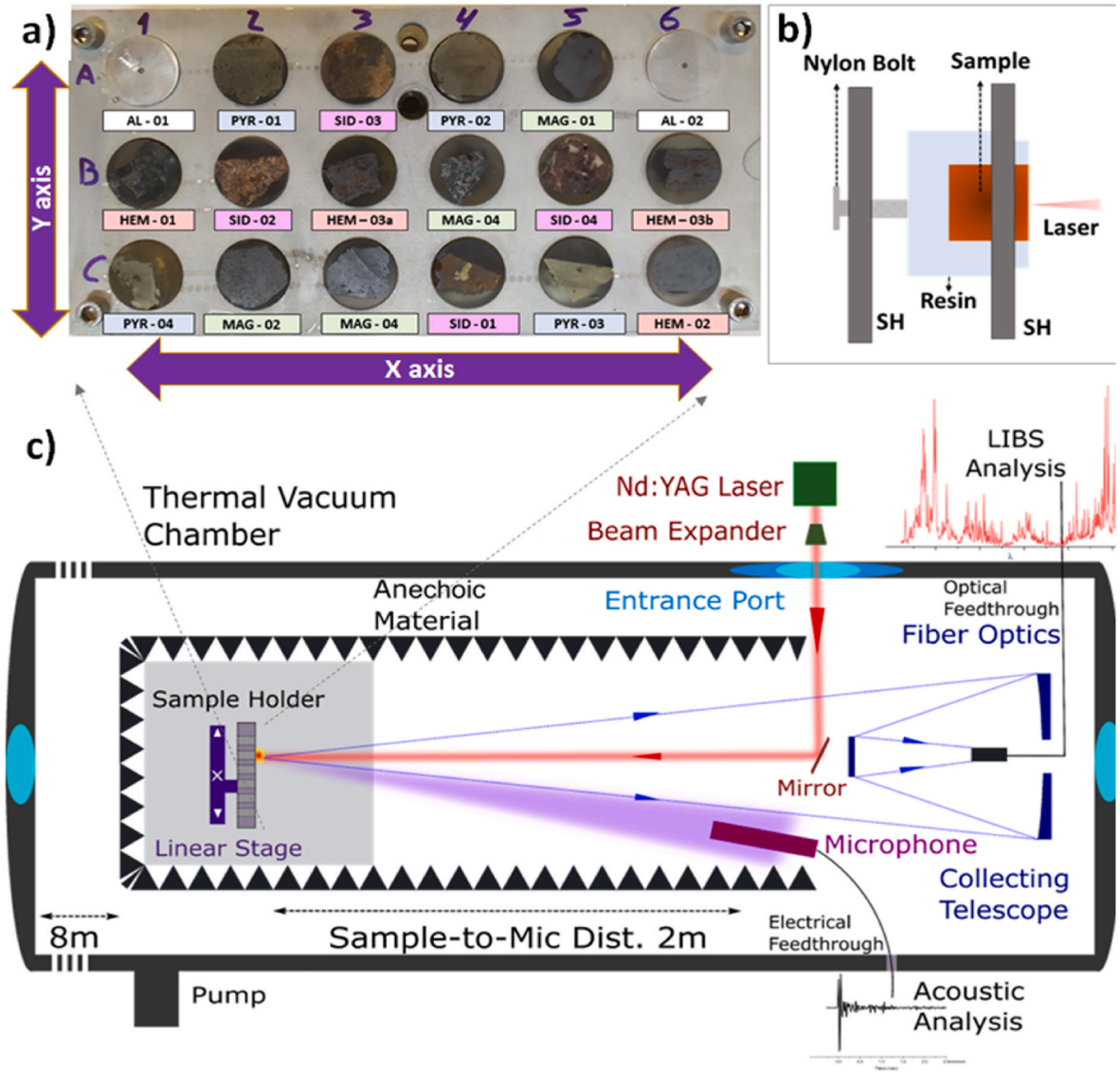

Fig. 1. a) Front-view of the sample holder fully loaded before experiments were performed. The labeling corresponds to the one shown in Table 1 b) Detail of the sample fixation on the sample holder. c) Top-view schematic representation of the experimental system used.

2. Experimental

2.1. Experimental set-up

The thermal vacuum chamber (TVC) used in the present work allowed to test the samples' acoustic response in remote configuration under atmospheric conditions mirroring those of Earth and Mars (1000 mbar, air, 295 K; 7 mbar, >96% CO_2, 245 K; respectively). A full description of the TVC can be found elsewhere [13]. For sample excitation, a pulsed Nd:YAG laser ($\lambda = 1064$ nm, $E_{pulse} = 80$ mJ, $\tau = 4$ ns) located outside the TVC was used.

Samples were placed in the custom-built holder shown in Fig. 1a, consisting of two aluminum plates. The holder allowed for up to 18 cylindrical samples to be placed at once, fixed using nylon bolts to keep their position (Fig. 1b). Moreover, the sample holder was mounted upon a XY motorized linear stage to refresh the sampling position.

The sample holder is positioned with its longest side longitudinally to the short axis of the chamber, allowing to change the sampling position between columns 1–6 (x-axis of the linear stage in Fig. 1c). In addition, the samples surfaces are mounted perpendicular to the laser path. The y-axis on the linear stage in Fig. 1c corresponds to vertical displacement, allowing to change the sampling position between rows A-C of the sample holder.

An hyper-cardioid condenser microphone (t.bone EM 9900, 20.8 mV Pa^{-1}) was used to record the laser-induced acoustic signal, digitalized using a 24-bit audio interface at a sampling rate of 96 kHz (UA-55 Quad-capture, Roland). To minimize the interferences due to reflections with the inner walls of the TVC, the sample holder was allocated inside a custom-built rectangular hemi-anechoic chamber covered with sound absorbent foam (HiLo-N40 polyurethane). Furthermore, a 0.5 m diameter anechoic tunnel was installed to insulate the full acoustic path (2-m long) from the plasma to the microphone, Fig. 1c.

For LIBS detection, emission from the plasma was collected by a 6' Ritchey-Chrétien telescope located at 2.5 m from the sample and directed into a 1 mm optical fiber integrated within the telescope. The optical fiber was connected to a time-integrated spectrometer (Avantes) located outside the TVC providing a resolution of 0.09–0.07 nm $pixel^{-1}$ depending on the wavelength. Spectra (250–460 nm) were collected with an acquisition delay time of 0.3 μs and 1 ms integration time.

2.2. Samples

A total of 15 mineral samples considered for the experiments, are described in Table 1, involved 3 sets of four homologues each for the same mineral specimen (pyrite, siderite, and magnetite) and one set of three hematite mineral homologues (been HEM-03 split in 2 fragments), all of them from different geographical origins.

Table 1
Mineral sample set used, as well as the geographic origin (if known) and the coordinate position in the sample holder.. Labelled as PYR – Pyrite; HEM – Hematite; SID – Siderite, and MAG - Magnetite.

Label	Origin	Pos.	Label	Origin	Pos.
PYR-01	Peru	A2	SID 001	Sierra Nevada, Granada, Spain	C4
PYR-02	Ambasaguas, Rioja, Spain	A4	SID 002	Galiarta, Bizkaia, Spain	B2
PYR-03	Navajun, Rioja, Spain	C5	SID 003	Troya-Mutiloa, Gipuzkoa, Spain	A3
PYR-04	Asturias, Spain	C1	SID 004	Unknown	B5
HEM 001	Bizkaia, Spain	B1	MAG 001	USA	A5
HEM 002	Unknown	C6	MAG 002	Burguillos del Cerro, Badajoz, Spain	C2
HEM 003a	Unknown	B3	MAG003	Cala, Huelva, Spain	C3
HEM 003b		B6	MAG004	Unknown	B4

The mineral samples were cut, polished and embedded in epoxy resin to conform cylindrical pieces (25 mm in ∅ × 15 mm). The samples were randomly distributed within the sample holder. Furthermore, 2 identical aluminum cylinders were located at the upper corner positions of the holder and were used as controls.

A total of 6 fresh positions at the target surface was sampled, inducing 50 plasma events at each position, thus generating a batch of 300 dual LIBS + audio files per sample.

2.3. Data processing

LIBS spectra were normalized via unity vector normalization after background subtraction following guidelines described in previous works [13]. At each sampling position, 50 plasma events were collected. The audio recordings containing every acoustic response were divided in 3 ms sections, each one containing an individual laser event. When applicable, the total area under the curve was considered to normalize frequency spectra. Raw LIBS data and acoustic frequency spectra, represented by the power spectral density estimation (300 Hz–27.5 kHz), were treated using MATLAB 2020b (Mathworks Inc.).

To compute any (dis-)similarity between either acoustic or LIBS spectra, the Euclidean and cosine distances were considered.

The cosine distance, defined as:

$$d_{ij} = 1 - x_i x'_j \left((x_i x'_i)(x_j x'_j) \right)^{-1/2}$$

conveys a relative comparison of two spectra (vectors x_i and x_j) by computing the cosine of the angle in the λ-dimensional space, providing a distance independent from the total magnitude of the spectrum.

In contrast, the Euclidean distance, defined as:

$$d_{ij} = \sqrt{(x_i - x_j)(x_i - x_j)'}$$

conveys an absolute comparison of two spectra, since this distance corresponds to the difference of their coordinates, that is, the length of the vector linking two spectral points in the λ-dimensional space. For both distance types, the larger the distance, the lower the similarity between the compared entities.

Finally, a partial least-squares (PLS) model was used as a self-consistent classifier. PLS is a well-known multivariate technique developed to model the relationship between a block of predictor variables (X) and another set of response variables (Y). The versatility of this algorithm allows its use to predict discrete/categorical variables [14]. Then, by calculating the variable importance in projection (VIP) score of each X-variable in the PLS, we can rank the variables with respect to their performance for discriminating between groups [15]. In general, variables with a VIP-score greater than 1 are considered important.

3. Results and discussion

3.1. Data exploration

3.1.1. Results using LIBS exclusively

Since the heterogeneous samples considered in this study were not expected to contain the pure mineral phases, an evaluation of the similarity between LIBS spectra, aimed to provide a qualitative picture of the studied homologues, was considered necessary. Therefore, an exploratory data analysis, based on the Euclidean and cosine distances, was conducted as follows:

At level 1, each sampling position was represented by the average spectrum of the 50 spectra collected at that position (centroid). The single distances of each spectrum to its centroid were calculated, resulting in 50(shots) × 6(positions) × 4(homologue) distances for the same mineral phase. The median of these distances defined the intra-position similarity.

At level 2, each mineral phase homologue became represented by the 6 LIBS spectra corresponding to the average spectra of each sampling position. From these sets of 6 average spectra, a single centroid was estimated and the distances of each representative spectrum to its particular centroid were calculated (6 × 4 distances for the same mineral phase). The median of these distances defined the inter-position similarity.

At level 3, each mineral phase became represented by 4 LIBS spectra, corresponding to the average spectra of each homologue. From these average spectra, a centroid was established for the entire mineral phase and the distances of the average spectra to that centroid were calculated (4 distances for the same mineral phase). The median of these distances defined then the inter-homologues similarity.

Finally, at level 4, each mineral phase became represented by a single LIBS spectrum, corresponding to the average spectrum of the 4 spectra characterizing its corresponding homologues defining its centroid. The distances from that centroid to the centroids associated with the rest of the mineral phases were calculated. The median of the obtained distances categorized the inter-minerals similarity.

Results for cosine and Euclidean distances are shown in Fig. 2a–b. As seen, the expected trend: intra-position < inter-position < inter-homologues < inter-minerals was observed for both distances. The most compromising situation was manifested by magnetite, as the results displayed almost similar inter-homologues and inter-phase distance values. In contrast, the LIBS spectra of pyrite, siderite, and hematite manifest sufficient representativeness to differentiate among the minerals.

A deeper exploration of the LIBS-based similarity was conducted via PCA to evaluate the potential clustering of a given mineral phase and their difference to the other phases. Unity-vector normalized LIBS spectra for each sampling position were used to compute the principal components scores. The score values for the first 3 principal components (total explained variance = 97%) are plotted in Fig. 2c. Results suggested a clustering of the different mineral phases, although the clustering for magnetite was particularly poor. A plausible explanation for this observation may be the contribution of emission lines linked to elements outside the expected mineral chemical formulae, i.e., impurities. Indeed, according to Anthony et al. [16], magnetite may feature minor contributions from oxides of Si, Mg and Ca – detected in our LIBS spectra– due to its association with silicates, quartz, apatite and others. Similarly, siderite can also present low concentrations of MgO and CaO and may appear associated with quartz, fluorites, or pyrites. Meanwhile, pyrite usually appears associated with other sulfides and sulfosalts, in addition to fluorite, calcite or quartz. Fig. 2d shows the representative LIBS spectrum for each mineral phase under study. The featuring of emission signals, represented in dashed lines, of Mg (Mg II ca. @280 nm and Mg I @285.2 nm) and Si (Si I @288.2 nm) point to the occurrence of these elements with higher prominence in siderite and magnetite, the latter also featuring emissions of Ca (e.g. Ca II @393.4 nm and @396.8 nm) and Ti lines (Ti I around 330 nm). These results corroborate that some compositional differences exist in the mineral phases, which are expected to induce some variability in the physical and chemical properties of the different samples under inspection. Yet, the random occurrence of these differences renders them poorly reliable for classification schemes.

3.1.2. *Laser-induced acoustics for mineral phase differentiation*

The absolute value between the maximum and the minimum of the first prominent peak in the time domain waveform (peak-to-peak amplitude) was monitored to process the acoustic recordings. Fig. 3a shows the average peak-to-peak acoustic amplitude, containing the data from all 6 positions sampled for each homologue within the four inspected mineral families. Pyrite homologues yielded the largest acoustic signal, with siderite homologues resulting in the lowest and

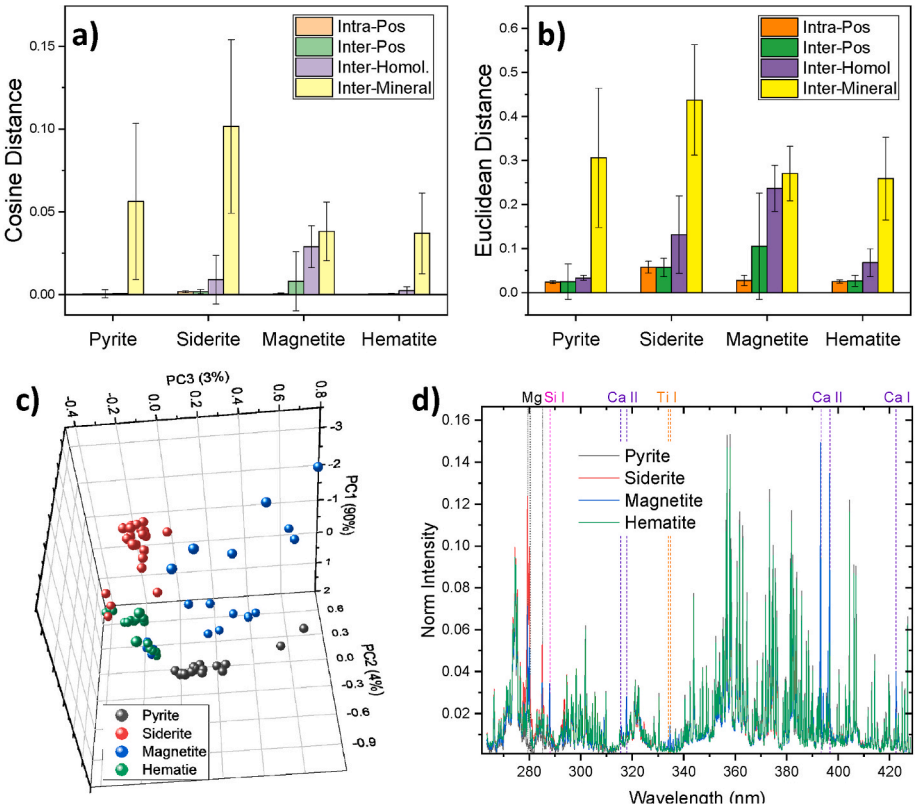

Fig. 2. a-b) Cosine and Euclidean distances for the four mineral phases, showing the Intra-position, Inter-position, Inter-homologue, and Inter-Mineral dissimilarities. c) PCA score values for each sampling position obtained from the normalized LIBS spectra. d) Average LIBS spectra for the studied mineral phases with non-Fe elemental lines highlighted.

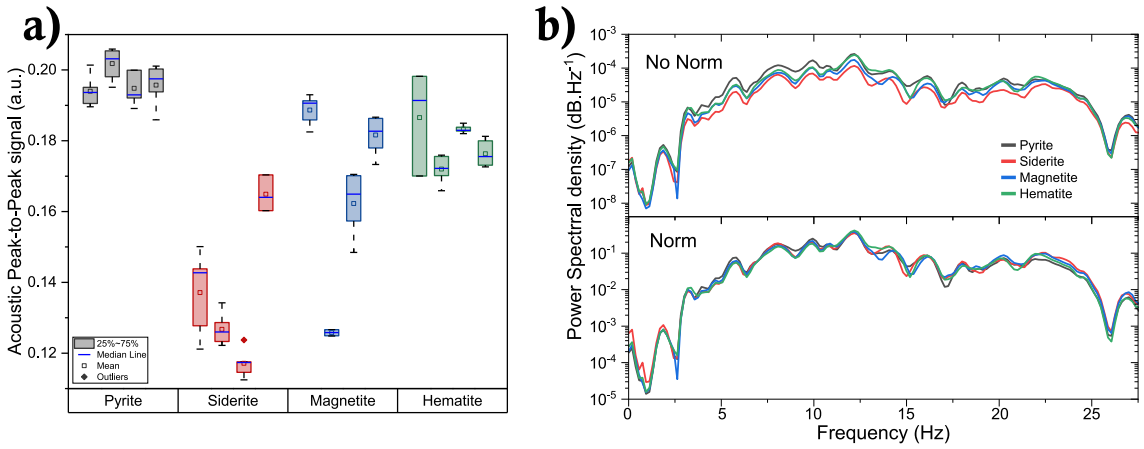

Fig. 3. a) Boxplot representing the average amplitude of the laser-induced acoustic signal for each homologue of the four different mineral phases. b) Non-normalized frequency domain power spectra for the mineral phases under study.

magnetite and hematite homologues featuring intermediate values. Moreover, pyrite and hematite provided the most consistent amplitude values, whereas siderite and magnetite were characterized by dispersed inter-homologue signals.

These results were in agreement with the observations from LIBS data shown in Fig. S1, where optical responses are displayed as the total emission intensity recorded. A parallelism can be observed in the behavior of both signals, even though there is not a complete correlation. According to literature, the acoustic signal is closely related to ablated mass during the ablation process [6]; for LIBS, however, the various processes related to plasma emission may cause a lack of correlation.

Spectral similarities in the acoustic frequency domain were also evaluated. The total area normalization aimed to eliminate the influence of variations in signal amplitude due to the nature of each mineral phase (Fig. 3a) and to reveal potential dissimilarities between minerals owing to the frequency content. Fig. 3b compares the non-normalized and normalized averaged power spectra for the mineral phases. Minute differences were evidenced when data were normalized; therefore, a detailed multivariate study was carried out to evaluate similarity.

Fig. 4a–b shows the cosine (for raw frequency data, since it does not depend on the signal magnitude) and Euclidean distances (for normalized frequency data) calculated for the acoustic responses at the same four levels explored previously. For comparative purposes, the distance value from the mineral phases to the aluminum targets is represented, as they were completely different both in composition and in traits. No matter the applied processing scheme, spectral similarity decreased from intra-position to inter-minerals scenarios, that is, as the conditions for acoustic recording were further varied. In general, the inter-homologue distances were smaller than the corresponding inter-mineral ones. As expected, the aluminum-to-targets average distance was larger than any of those computed using the mineral samples. This

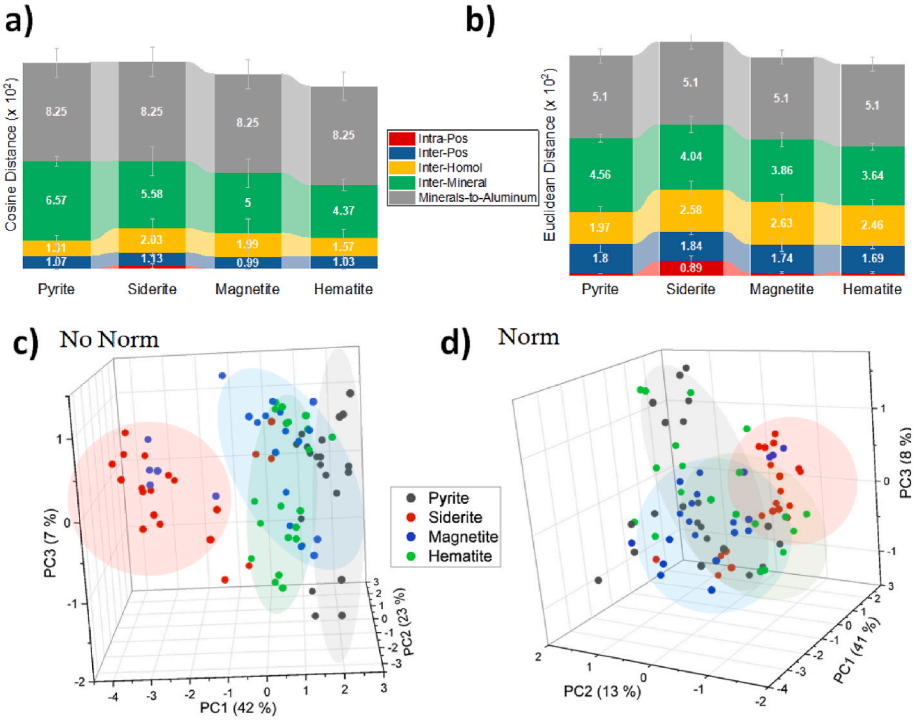

Fig. 4. a-b) Cosine and Euclidean distances for the four mineral phases, showing the intra-position, inter-position, inter-homologues, and inter-minerals dissimilarities. c-d) PCA score values for each sampling position obtained from the non-normalized (c) and normalized frequency spectra (d).

observation suggests that frequency spectra provide information related to the mineral phase itself.

It is worth noting that, even though targets were distributed randomly along the sample holder, some spectral interferences due to the experimental configuration were found when probing the aluminum cylinders (A1 and A6 in Fig. 1a). Fig. S2 presents the frequency spectra recorded for both Al samples. Within a same sample, effects due to changes in the sampling position were observed. Further differences, remarkably in the 12–18 kHz region, were found to arise upon changing the location in the sample holder. Because the sample-to-surroundings distance was kept constant, the interaction between the acoustic wave and the sample holder seems to be the source of these interferences.

Finally, a PCA was performed. The scores of the first 3 PCs for the 16 inspected samples are plotted in Fig. 4. From non-normalized data (Fig. 4c), pyrite, siderite and hematite could be differentiated. In contrast, normalized data (Fig. 4d) showed higher dispersion even if a slight tendency towards clustering was hinted. The behavior for non-normalized spectra, mainly explained by PC1, was analogous to that observed in Fig. S3 as pyrite and siderite displayed contrary values whereas magnetite and hematite were similar, indicating that the amplitude of the acoustic wave partially governed data separation. On the contrary, this contribution was absent from results in Fig. 4d, while the impact of the variability introduced by spectral interferences was more prominent. Although the plotted scores did not allow for a clear mineral clustering, they strongly suggested the existence of valuable information within the acoustic response. Yet, this information was convoluted with the contributions of the aforementioned interference patterns.

3.2. *One-vs-all frequency data inspection to differenciate mineral phases*

To further explore the usefulness of frequency data for mineral differentiation, the acoustic frequency spectra were employed to build PLS *one-vs-all* classification models. The X matrix included the frequency spectra, while the Y matrix values were defined as +1 for samples belonging the group under study and −1 for the rest. Thus, 4 PLS models were built (one for each mineral group). Fig. 5a shows the scores plot of the two first latent variables for each PLS model. The scores plot, no matter the model, allowed for straightforward visualization of the labelled group with regards to the rest of the groups. The VIP-scores for the PLS models and predictors (frequency values) that contribute the most to variance explanation for a selected PLS model variable are revealed in Fig. 5b. The most contributive variables are highlighted by blue dots. To increase the accuracy of the results, an iterative method (n = 2000 iterations) randomly selected 80% of the average acoustic spectra for each sampling position each time. As a criterion, the final value (cutoff threshold) to any VIP score considered relevant (and, thus, the frequency variable) after 2000 iterations should amount to the unit plus two times its standard deviation.

Fig. S4 from Supplementary Material shows that, in most of the cases, the most important variables were closely correlated to the highest factor weights for the first two latent variables of the PLS models.

3.3. *Frequency analysis for mineral discrimination in Martian atmosphere*

SuperCam's microphone on board the Perseverance rover is the most ambitious attempt to combine in-field LIBS and acoustic measurements. Due to the many uncontrollable variables impacting the records, in-field acoustic analysis is an intricate topic. Still, deepening the insight on how the Martian atmospheric composition affects the described results may further validate the current data analysis scheme and highlight its use for future studies. Thus, in this context, the applicability of the developed frequency-based scheme was evaluated, under a simulated Martian environment. The Martian atmosphere conforms a remarkably different medium for the transmission of acoustic waves owing to its composition, temperature and pressure [17,18]; resulting in a slower speed of sound and weaker acoustic waves owing to the frequency absorption profile of the atmosphere. From the acoustic point of view, as the properties of the atmosphere change, the propagation of sound waves varies accordingly. Subsequently, variations in the absorption coefficient for each frequency and the formed interference patterns may mask frequency ranges of relevance under terrestrial conditions and unravel others previously obscured. Furthermore, it is essential to remark that the sound source is different in both scenarios. The laser-induced plasma evolution radically changes under low-pressure conditions and atmosphere composition. Previous studies have highlighted benefits derived from using LIBS and acoustic data either by data fusion [13] or in correlation [11,12] under Earth and Mars-like environment, yet frequency spectra remain to be tested for similar purposes.

Following the PLS-based procedure, and choosing 3LV, scores and

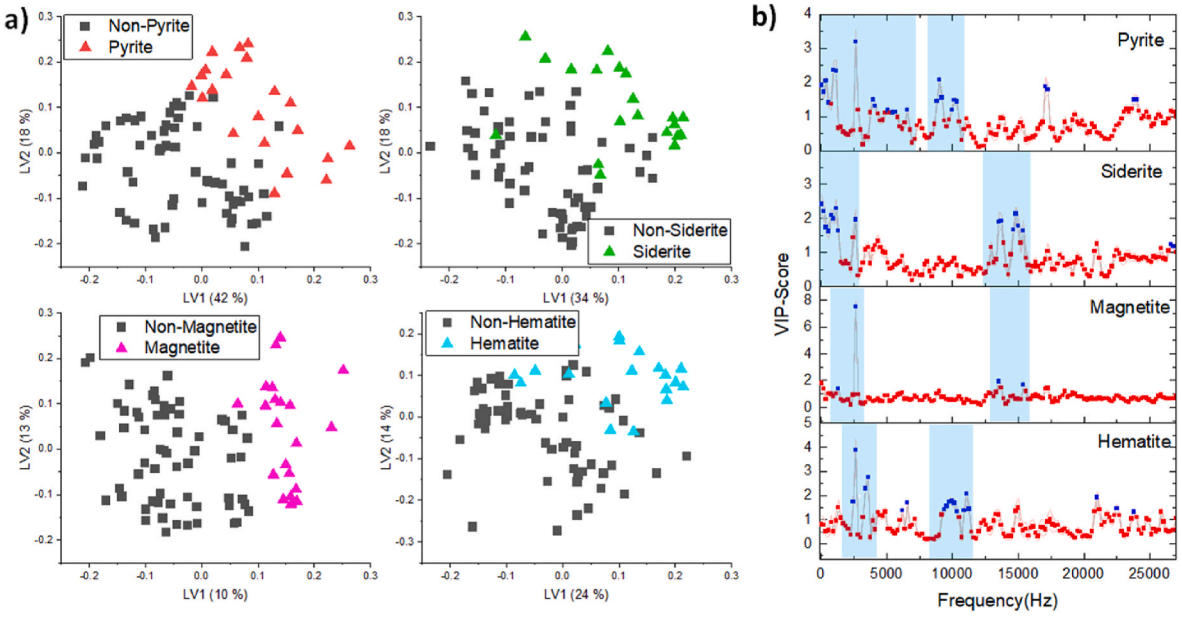

Fig. 5. *a) Score values for the 2 first LV for the 4 PLS-one-vs-all. b) VIP-Score values for each variable for the 4 PLS models. Blue dots represent the variables above the cutoff threshold.* (For interpretation of the references to colour in this figure legend, the reader is referred to the Web version of this article.)

VIP-scores for the four models are plotted in Fig. 6a–b. Significant variables were set again as those with value higher than $\overline{x} \pm 2SD$ after 2000 iterations. The differentiation between the studied mineral phases using only the frequency spectra was also proved in Mars-like atmosphere. Under Martian atmosphere the frequency ranges between 10 and 14 kHz seemed to be significant for every sample, albeit with slight variations. However, the power spectral density in this range was several orders of magnitude lower due to the acoustic absorption caused by the Mars-like atmosphere. Thus, we cannot discard that those frequencies were part from an interference pattern generated by reflections of the lower frequencies close to the microphone and detected later.

3.4. Acoustic frequency signal and optical response for classification of minerals

Lastly, the capability of LIBS and the recorded frequencies for sample classification was tested independently to expand on the reported results. LIBS results were used as reference values to compare the performance of the acoustic-based approach. From results described above, it was reasonable to expect that acoustic-based discrimination underperformed when compared to LIBS. However, when pairing the results from both approaches, the degree of "acoustic spectral signature" within the recorded acoustic signal compared to LIBS spectra may be hinted.

We based the classification model on PLS, setting the Y matrix to a 4-column multi-response matrix where the values in each column are set as either +1 or −1 depending on whether the sampled belonged or not to a given mineral phase [19]. For acoustic data, 7 LV were chosen. To compute the prediction value, the samples were split in two sets, a training one and a validation one (67% and 33% of the total samples). An iterative process (5000 iterations) was run with each successive loop designing the matrices randomly.

The number of LVs in each model has been chosen by optimizing the average hit-rate after 5000 iterations. The hit-rate was calculated on the validation matrix (1/3 of the sample number) by averaging the results of all iterations. Finally, the number of samples correctly assigned in each iteration was averaged, thus yielding individual values displayed in Table 2. To confirm that the classification scheme was non-biased due to interferences or other factors, the same process was repeated by assigning random groups, with the hit-rate decreasing to 24%.

Table 2
Classification hit rate after 5000 iterations for the studied mineral phases.

	Norm (%)	No-Norm (%)	LIBS
Mars	64	75	93
Earth	78	83	95

As expected, a lower predictive performance was observed for acoustic data. Nonetheless, these results complement those obtained previously, indicating the presence of mineralogical information in the acoustic frequency spectrum. It is interesting to point out that the raw frequency signals provided higher hit rates than normalized data. Moreover, the classification of mineral specimens under Martian setting seemed more complicated than in Earth. However, with values hovering around 80%, it is possible to unequivocally rely on frequency spectra containing sample-related information even if it is not as readily accessible as the emission lines in LIBS.

4. Conclusions

The present work explores the use of laser-induced plasma acoustic data in the frequency domain for the differentiation of mineral phases yielding highly similar LIBS emission spectra. We prove that the frequency spectra contain information related to the mineral phase composition, although the presence of interferences and echoes was more critical than in the case of LIBS. Four different Fe-based mineral phases, with several homologues from distinct geographical origins, were used to study the occurrence of interferences due to the sample surroundings.

In the first place, mineral differentiation using LIBS and acoustic data was tested by employing the cosine and Euclidean distances and PCA to establish a reference to which frequency data could be compared. The similarity degree was computed for both data sources, indicating that

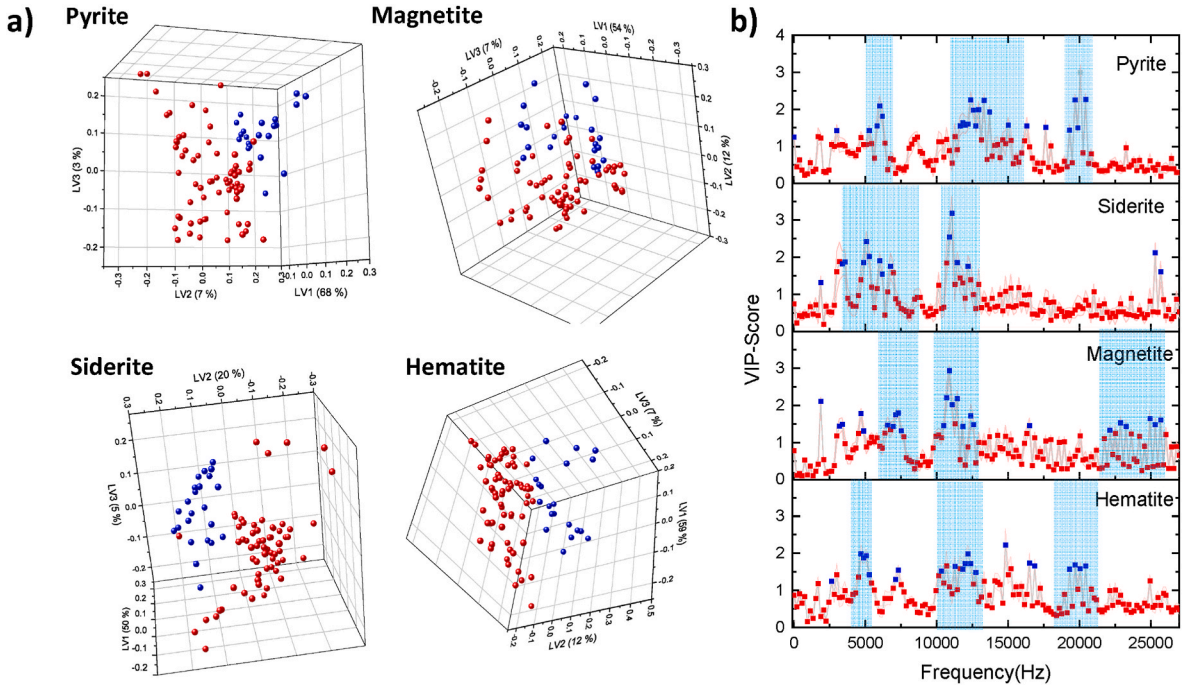

Fig. 6. a) Score values for the 3 LV variables for the 4 PLS one-vs-all models. Blue dots represent the +1 phase for each model. b) VIP-Score values for each variable for the 4 PLS models. Blue dots represent the variables above the cutoff threshold. (For interpretation of the references to colour in this figure legend, the reader is referred to the Web version of this article.)

the spectra obtained by both approaches were less similar between different mineral phases than among samples belonging to the same mineral phase. These observations point to the potential of using frequency spectra as an added information layer when the acquired optical spectra predominantly exhibit the same lines.

Furthermore, a one-vs-all PLS method was successfully used to verify the capabilities of frequency data to correctly allocate replicas within the same group based on physical traits differences existing between families. Normalized acoustic spectra allowed finding differences between a specific mineral phase and the others. The use of VIP-score made it possible to identify spectral ranges that seemed to provide a better separation in the PLS score 2D-space, which could represent traits specific to each mineral phase. The TVC used herein enabled performing our analyses under two very different acoustic propagation media, Earth atmosphere and Mars-like environment, to test the robustness and general applicability of the data acquisition and processing schemes reported herein. Frequency-based mineral differentiation under Martian conditions was also successful, owing to characteristic signals in the 10–14 kHz window, highlighting possible future uses of laser-induced plasma acoustics. Finally, the use of the acoustic signal to perform a discriminatory analysis allowed to obtain results similar to those yielded by LIBS (80% vs. 95% hit rate), confirming the existence of specific information highly representative of the mineral phase in the acoustic response.

This work constitutes the first attempt to use laser-produced plasma acoustics in the frequency domain for mineral phases discrimination to the best of our knowledge. While apparent limitations such as difficulties in eliminating interferences were present, we demonstrate that these spectra can expand the description of the sample when performed alongside LIBS.

CRediT authorship contribution statement

César Alvarez-Llamas: Conceptualization, Investigation, Methodology, Software, Formal analysis, Writing – original draft, Writing – review & editing. **Pablo Purohit:** Conceptualization, Investigation, Methodology, Writing – original draft, Writing – review & editing. **Javier Moros:** Conceptualization, Writing – review & editing, Funding acquisition. **Javier Laserna:** Conceptualization, Writing – review & editing, Supervision, Project administration, Funding acquisition, All authors revised and contributed to the manuscript and have given approval to the final version of the manuscript.

Declaration of competing interest

The authors declare the following financial interests/personal relationships which may be considered as potential competing interests: Javier Laserna reports financial support was provided by Junta de Andalucia, Spain. Javier Laserna reports financial support was provided by Spain Ministry of Science and Innovation. Pablo Purohit reports financial support was provided by Spain Ministerio de Universidades. Javier Laserna reports a relationship with Spain Ministry of Science and Innovation that includes: funding grants.

Data availability

Data will be made available on request.

Acknowledgments

This work was supported by the projects UMA18-FEDERJA-272 (Junta de Andalucía) and PID2020-119185GB-I00 (Ministerio de Ciencia e Innovación, Spain). P.P. is grateful to the European Union's NextGenerationEU plan and the Spanish Ministerio de Universidades for his Margarita Salas fellowship under the program "Ayudas para la recualificación del Sistema Universitario español". Funding for open access charge: Universidad de Málaga/CBUA.

Appendix A. Supplementary data

Supplementary data to this article can be found online at https://doi.org/10.1016/j.aca.2022.340261.

References

[1] D. V S, S. D. George, V. B. Kartha, S. Chidangil, and U. V K, "Hybrid LIBS-Raman-LIF systems for multi-modal spectroscopic applications: a topical review," Appl. Spectrosc. Rev., 56, 6, 463-491, 2021, 10.1080/05704928.2020.1800486.
[2] J. Laserna, J.M. Vadillo, P. Purohit, Laser-induced breakdown spectroscopy (LIBS): fast, effective, and agile leading edge analytical technology, Appl. Spectrosc. 72 (1_suppl) (2018) 35–50, https://doi.org/10.1177/0003702818791926.
[3] E. Gibbons, R. Léveillé, and K. Berlo, "Data fusion of laser-induced breakdown and Raman spectroscopies: enhancing clay mineral identification," Spectrochim. Acta Part B At. Spectrosc., 170, June,105905, 2020, 10.1016/j.sab.2020.105905.
[4] J. Moros, M.M. Elfaham, J. Laserna, Dual-spectroscopy platform for the surveillance of Mars mineralogy using a decisions fusion architecture on simultaneous LIBS-Raman data, Anal. Chem. 90 (3) (2018) 2079–2087, https://doi.org/10.1021/acs.analchem.7b04124.
[5] F. Anabitarte, L. Rodríguez-Cobo, J.-M. López-Higuera, A. Cobo, Normalization of laser-induced breakdown spectroscopy spectra using a plastic optical fiber light collector and acoustic sensor device, Appl. Opt. 51 (34) (2012) 8306–8314, https://doi.org/10.1364/AO.51.008306.
[6] S. Kradolfer, K. Heutschi, J. Koch, D. Günther, Tracking mass removal of portable laser ablation sampling by its acoustic response, Spectrochim. Acta Part B At. Spectrosc. 179 (2021), 106118, https://doi.org/10.1016/j.sab.2021.106118.
[7] S. Maurice, et al., The SuperCam instrument suite on the Mars 2020 rover: science objectives and mast-unit description, Space Sci. Rev. 217 (3) (2021), https://doi.org/10.1007/s11214-021-00807-w, 47.
[8] S. Maurice, et al., In situ recording of Mars soundscape, Nature (Apr. 2022), https://doi.org/10.1038/s41586-022-04679-0.
[9] N. Murdoch, et al., Laser-induced breakdown spectroscopy acoustic testing of the Mars 2020 microphone, Planet. Space Sci. 165 (September 2018) 260–271, https://doi.org/10.1016/j.pss.2018.09.009, 2019.
[10] B. Chide, et al., Listening to laser sparks: a link between Laser-Induced Breakdown Spectroscopy, acoustic measurements and crater morphology, Spectrochim. Acta Part B At. Spectrosc. 153 (2019) 50–60, https://doi.org/10.1016/j.sab.2019.01.008, 2018.
[11] B. Chide, et al., Acoustic monitoring of laser-induced phase transitions in minerals: implication for Mars exploration with SuperCam, Sci. Rep. 11 (1) (2021), https://doi.org/10.1038/s41598-021-03315-7, 24019.
[12] B. Chide, et al., Recording laser-induced sparks on Mars with the SuperCam microphone, Spectrochim. Acta Part B At. Spectrosc. 174 (2020), https://doi.org/10.1016/j.sab.2020.106000.
[13] C. Alvarez-Llamas, P. Purohit, J. Moros, J. Laserna, LIBS-acoustic mid-level fusion scheme for mineral differentiation under terrestrial and martian atmospheric conditions, Anal. Chem. 94 (3) (2022) 1840–1849, https://doi.org/10.1021/acs.analchem.1c04792.
[14] R. Brennetot, Applied Chemometrics for Scientists, John Wiley & Sons, 2007.
[15] I.-G. Chong, C.-H. Jun, Performance of some variable selection methods when multicollinearity is present, Chemometr. Intell. Lab. Syst. 78 (1–2) (2005) 103–112, https://doi.org/10.1016/j.chemolab.2004.12.011.
[16] J.W. Anthony, R.A. Bideauz, K.W. Blath, N.C. Nichols (Eds.), Handbook of Mineralogy, Mineralogical Society of America, 2002.
[17] A. Petculescu, Acoustic properties in the low and middle atmospheres of Mars and Venus, J. Acoust. Soc. Am. 140 (2) (2016) 1439–1446, https://doi.org/10.1121/1.4960784.
[18] H.E. Bass, J.P. Chambers, Absorption of sound in the Martian atmosphere, J. Acoust. Soc. Am. 109 (6) (2001) 3069–3071, https://doi.org/10.1121/1.1365424.
[19] R. Brennetot, Chemometrics for Pattern Recognition, John Wiley & Sons, 2009.